

Spin-Orbit Coupling, Antilocalization, and Parallel Magnetic Fields in Quantum Dots

D. M. Zumbühl,¹ J. B. Miller,^{1,2} C. M. Marcus,¹ K. Campman,³ and A. C. Gossard³

¹Department of Physics, Harvard University, Cambridge, Massachusetts 02138

²Division of Engineering and Applied Sciences, Harvard University, Cambridge, Massachusetts 02138

³Department of Electrical and Computer Engineering, University of California, Santa Barbara, California 93106

(Received 22 August 2002; published 18 December 2002)

We investigate antilocalization due to spin-orbit coupling in ballistic GaAs quantum dots. Antilocalization that is prominent in large dots is suppressed in small dots, as anticipated theoretically. Parallel magnetic fields suppress both antilocalization and also, at larger fields, weak localization, consistent with random matrix theory results once orbital coupling of the parallel field is included. *In situ* control of spin-orbit coupling in dots is demonstrated as a gate-controlled crossover from weak localization to antilocalization.

DOI: 10.1103/PhysRevLett.89.276803

PACS numbers: 73.23.Hk, 73.20.Fz, 73.50.Gr

The combination of quantum coherence and electron spin rotation in mesoscopic systems produces a number of interesting transport properties. Numerous proposals for potentially revolutionary electronic devices that use spin-orbit (SO) coupling have appeared in recent years, including gate-controlled spin rotators [1] as well as sources and detectors of spin-polarized currents [2]. It has also been predicted that the effects of some types of SO coupling will be strongly suppressed in small 0D systems, i.e., quantum dots [3–5].

In this Letter, we investigate SO effects in ballistic-chaotic GaAs/AlGaAs quantum dots. We identify the signature of SO coupling in ballistic quantum dots to be *antilocalization* (AL), leading to characteristic magneto-conductance curves, analogous to known cases of disordered 1D and 2D systems [6–11]. AL is found to be prominent in large dots and suppressed in smaller dots, as anticipated theoretically [3–5]. Results are generally in excellent agreement with a new random matrix theory (RMT) that includes SO and Zeeman coupling [5]. Moderate magnetic fields applied in the plane of the 2D electron gas (2DEG) in which the dots are formed cause a crossover from AL to weak localization (WL). This can be understood as a result of Zeeman splitting, consistent with RMT [5]. At larger parallel fields WL is also suppressed, which is not expected within RMT. The suppression of WL is explained by orbital coupling of the parallel field, which breaks time-reversal symmetry [12]. Finally, we demonstrate *in situ* electrostatic control of the SO coupling by tuning from AL to WL in a dot with a center gate.

In mesoscopic conductors, coherent backscattering of time-reversed electron trajectories leads to a conductance *minimum* (WL) at $B = 0$ in the spin-invariant case, and a conductance *maximum* (AL) in the case of strong SO coupling [6]. In semiconductor heterostructures, SO coupling results mainly from electric fields [13] (appearing as magnetic fields in the electron frame), leading to momentum dependent spin precessions due to crystal

inversion asymmetry (Dresselhaus term [14]) and hetero-interface asymmetry (Rashba term [15]).

SO coupling effects have been previously measured using AL in GaAs 2DEGs [8–10] and other 2D heterostructures [11]. Other means of measuring SO coupling in heterostructures, such as from Shubnikov–de Haas oscillations [16] and Raman scattering [17] are also quite developed. SO effects have also been reported in

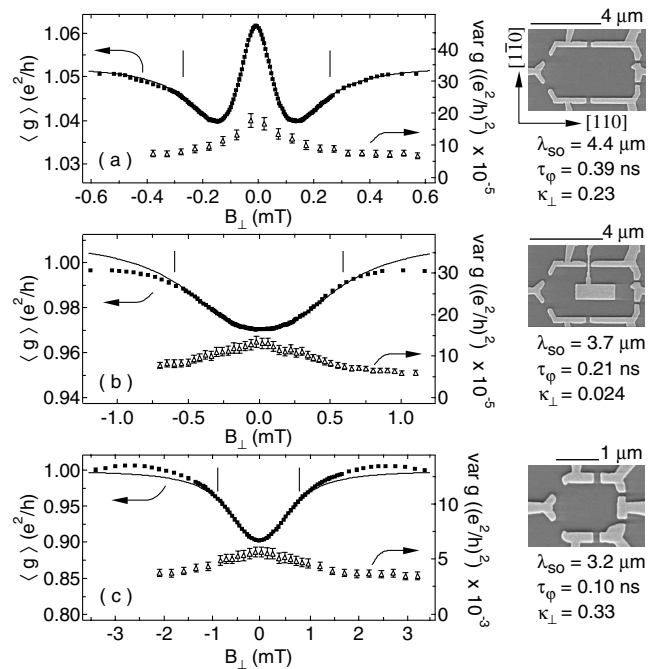


FIG. 1. Average conductance $\langle g \rangle$ (squares) and variance of conductance $\text{var}(g)$ (triangles) calculated from ~ 200 statistically independent samples (see text) as a function of perpendicular magnetic field B_{\perp} for (a) $8.0 \mu\text{m}^2$ dot, (b) $5.8 \mu\text{m}^2$ center-gated dot, and (c) $1.2 \mu\text{m}^2$ dot at $T = 0.3 \text{ K}$, along with fits to RMT (solid curves). In (b), the center gate is fully depleted. Vertical lines indicate the fitting range; error bars of $\langle g \rangle$ are about the size of the squares.

TABLE I. Dot area $A = L_1 L_2$ (130 nm edge depletion); spin-degenerate mean level spacing $\Delta = 2\pi\hbar^2/m^*A$ ($m^* = 0.067m_e$); dwell time $\tau_d = h/(N\Delta)$; Thouless energy $E_T = \hbar v_F/\sqrt{A}$; $\epsilon_{\perp}^{\text{so}}/\Delta$ and $\epsilon_{\parallel}^{\text{so}}/\Delta$ for the fits in Fig. 1; B^6 coefficients a_1 and a_2 from one and two parameter fits; B^6 coefficient b_2 from two parameter fit; see text.

A	Δ	τ_d	E_T/Δ	$\epsilon_{\perp}^{\text{so}}/\Delta$	$\epsilon_{\parallel}^{\text{so}}/\Delta$	a_1, a_2	b_2
μm^2	μeV	ns				(ns) $^{-1}\text{T}^{-2}$	(ns) $^{-1}\text{T}^{-6}$
1.2	6.0	0.35	33	0.15	0.04	6.6, 6.6	0.24
5.8	1.2	1.7	73	0.32	0.33	3.2, 0	140
8	0.9	2.3	86	3.6	3.1	1.4, 0.9	3.7

mesoscopic systems such as Aharonov-Bohm rings, wires, and carbon nanotubes [18]. Recently, parallel field effects of SO coupling in quantum dots were measured [19,20]. The observed reduction of conductance fluctuations in a parallel field [20] was explained in terms of SO effects [4,5], leading to an extension of RMT to include new symmetry classes associated with SO and Zeeman coupling [5].

This RMT addresses quantum dots coupled to two reservoirs via N total conducting channels, with $N \gg 1$. It assumes $(\gamma, \epsilon_Z) \ll E_T$, where $\gamma = N\Delta/(2\pi)$ is the level broadening due to escape, Δ is the mean level spacing, $\epsilon_Z = g\mu_B B$ is the Zeeman energy, and E_T is the Thouless energy (Table I). Decoherence is included as a fictitious voltage probe [5,21] with dimensionless dephasing rate $N_{\varphi} = h/(\Delta\tau_{\varphi})$, where τ_{φ} is the phase coherence time. SO lengths $\lambda_{1,2}$ along respective principal axes [110] and $[1\bar{1}0]$ are assumed (within the RMT) to be large compared to the dot dimensions $L_{1,2}$ along these axes. We define the mean SO length $\lambda_{\text{so}} = \sqrt{|\lambda_1 \lambda_2|}$ and SO anisotropy $\nu_{\text{so}} = \sqrt{|\lambda_1/\lambda_2|}$. SO coupling introduces two energy scales: $\epsilon_{\perp}^{\text{so}} = \kappa_{\perp} E_T (L_1 L_2 / \lambda_{\text{so}}^2)^2$, representing a spin-dependent Aharonov-Bohm-like effect, and $\epsilon_{\parallel}^{\text{so}} \sim [(L_1/\lambda_1)^2 + (L_2/\lambda_2)^2] \epsilon_{\perp}^{\text{so}}$, providing spin flips. AL appears in the regime of strong SO coupling, $(\epsilon_{\perp}^{\text{so}}, \epsilon_{\parallel}^{\text{so}}) \gg \tilde{\gamma}$, where $\tilde{\gamma} = (\gamma + \hbar/\tau_{\varphi})$ is the total level broadening. Note that large dots reach the strong SO regime at relatively weaker SO coupling than small dots. Parameters λ_{so} , τ_{φ} , and κ_{\perp} (a factor related to trajectory areas) are extracted from fits to dot conductance as a function of perpendicular field, B_{\perp} . The asymmetry parameter, ν_{so} , is estimated from the dependence of magnetoconductance on parallel field, B_{\parallel} .

The quantum dots are formed by lateral Cr-Au depletion gates defined by electron-beam lithography on the surface of a GaAs/AlGaAs heterostructure grown in the [001] direction. The 2DEG interface is 349 Å below the wafer surface, comprising a 50 Å GaAs cap layer and a 299 Å AlGaAs layer with two Si δ -doping layers 143 and 161 Å from the 2DEG. An electron density of $n \sim 5.8 \times 10^{15} \text{ m}^{-2}$ [22] and bulk mobility $\mu \sim 24 \text{ m}^2/\text{Vs}$ (cooled in the dark) gives a transport mean free path $\ell_e \sim 3 \mu\text{m}$. This 2DEG is known to show AL in 2D [10].

Measurements were made in a ^3He cryostat at 0.3 K using current bias of 1 nA at 338 Hz. Shape-distorting gates were used to obtain ensembles of statistically independent conductance measurements [23] while the point contacts were actively held at one fully transmitting mode each ($N = 2$).

Figure 1 shows average conductance $\langle g \rangle$, and variance of conductance fluctuations, $\text{var}(g)$, as a function of B_{\perp} for the three measured dots: a large dot ($8 \mu\text{m}^2$), a variable size dot with an internal gate ($5.8 \mu\text{m}^2$ or $8 \mu\text{m}^2$, depending on center gate voltage), and a smaller dot ($1.2 \mu\text{m}^2$). Each data point represents ~ 200 independent device shapes. The large dot shows AL while the small and gated dots show WL. Estimates for λ_{so} , τ_{φ} , and κ_{\perp} , from RMT fits are listed for each device below the micrographs in Fig. 1 (see Table I for corresponding ϵ_{\perp} and ϵ_{\parallel}). When AL is present (i.e., for the large dot), estimates for λ_{so} have small uncertainties ($\pm 5\%$) and give upper and lower bounds; when AL is absent (i.e., for the small and gated dots) only a lower bound for λ_{so} (-5%) can be extracted from fits. The value $\lambda_{\text{so}} \sim 4.4 \mu\text{m}$ is consistent with all dots and in good agreement with AL measurements made on an unpatterned 2DEG sample from the same wafer [10].

Comparing Figs. 1(a) and 1(c), and recalling that all dots are fabricated on the same wafer, one sees that AL is suppressed in smaller dots, even though λ_{so} is sufficient to produce AL in the larger dot. We note that these dots do not strongly satisfy the inequalities $L/\lambda_{\text{so}} \ll 1, N \gg 1$, having $N = 2$ and $L/\lambda_{\text{so}} = 0.64$ (0.34) for the large (small) dot. Nevertheless, Fig. 1 shows the very good agreement between experiment and the new RMT.

We next consider the influence of B_{\parallel} on $\langle g \rangle$. In order to apply tesla-scale B_{\parallel} while maintaining subgauss control of B_{\perp} , we mount the sample with the 2DEG aligned to the axis of the primary solenoid (accurate to $\sim 1^\circ$) and use an independent split-coil magnet attached to the cryostat to provide B_{\perp} as well as to compensate for sample misalignment [20]. Figure 2 shows shape-averaged magnetoconductance (relative to $B_{\perp} \gg \phi_0/A$, i.e., fully broken time-reversal symmetry), $\delta g(B_{\perp}, B_{\parallel}) = \langle g(B_{\perp}, B_{\parallel}) \rangle - \langle g(B_{\perp} \gg \phi_0/A, B_{\parallel}) \rangle$ as a function of B_{\perp} at several values of B_{\parallel} , along with fits of RMT [5] with parameters λ_{so} , τ_{φ} , and κ_{\perp} set by a single fit to the $B_{\parallel} = 0$ data. The low-field dependence of $\delta g(0, B_{\parallel})$ on B_{\parallel} [Fig. 2(b)] allows the remaining parameter, ν_{so} , to be estimated as described below.

Besides Zeeman energy ϵ_Z (calculated using $g = -0.44$ rather than fit), parallel field combined with SO coupling introduces an additional new energy scale, $\epsilon_{\perp}^Z = [(\kappa_Z \epsilon_Z^2 A)/(2E_T)] \sum_{i,j=1,2} \frac{l_i l_j}{\lambda_i \lambda_j}$, where κ_Z is a dot-dependent constant and $l_{1,2}$ are the components of a unit vector along B_{\parallel} [5]. Because orbital effects of B_{\parallel} on $\delta g(B_{\perp}, B_{\parallel})$ dominate at large B_{\parallel} , ϵ_{\perp}^Z must instead be estimated from RMT fits of $\text{var}(g)$ with already broken time-reversal symmetry, which is unaffected by orbital coupling [24].

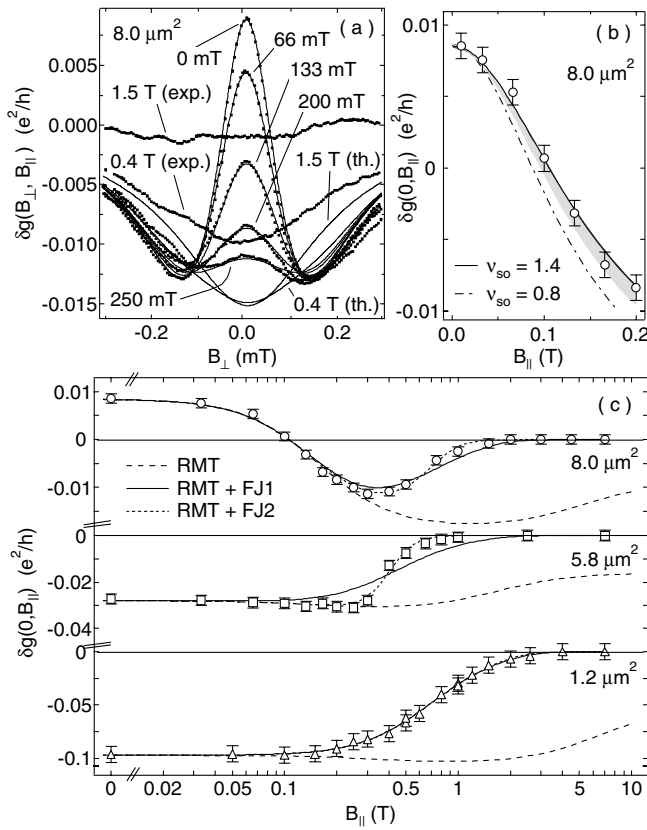


FIG. 2. (a) Difference of average conductance from its value at large B_{\perp} , $\delta g(B_{\perp}, B_{\parallel})$, as a function of B_{\perp} for several B_{\parallel} for the $8.0 \mu\text{m}^2$ dot at $T = 0.3 \text{ K}$ (squares) with RMT fits (curves). (b) Sensitivity of $\delta g(0, B_{\parallel})$ to ν_{so} for the $8.0 \mu\text{m}^2$ dot, $1 \leq \nu_{\text{so}} \leq 2$ (shaded), $\nu_{\text{so}} = 1.4$ (solid line), and $\nu_{\text{so}} = 0.8$ (dashed line). (c) $\delta g(0, B_{\parallel})$ (markers) with RMT predictions (dashed curves) and one parameter (solid curves) or two parameter fits (dotted curves) using RMT including a suppression factor due to orbital coupling of B_{\parallel} ; see text.

The RMT formulation [5] is invariant under $\nu_{\text{so}} \rightarrow r/\nu_{\text{so}}$, where $r = L_1/L_2$ [25], and gives an extremal value of $\delta g(0, B_{\parallel})$ at $\nu_{\text{so}} = \sqrt{r}$. As a consequence, fits to $\delta g(0, B_{\parallel})$ cannot distinguish between ν_{so} and r/ν_{so} . As shown in Fig. 2(b), data for the $8 \mu\text{m}^2$ dot ($r \sim 2$) are consistent with $1 \leq \nu_{\text{so}} \leq 2$ and appear best fit to the extremal value, $\nu_{\text{so}} \sim 1.4$. Values of ν_{so} that differ from one indicate that both Rashba and Dresselhaus terms are significant, which is consistent with 2D data taken on the same material [10].

Using $\nu_{\text{so}} = 1.4$ and values of λ_{so} , τ_{ϕ} , and κ_{\perp} from the $B_{\parallel} = 0$ fit, RMT predictions for $\delta g(B_{\perp}, B_{\parallel})$ agree well with experiment up to about $B_{\parallel} \sim 0.2 \text{ T}$ [Fig. 2(a)], showing a crossover from AL to WL. For higher parallel fields, however, experimental δg 's are suppressed relative to RMT predictions. By $B_{\parallel} \sim 2 \text{ T}$, WL has vanished in all dots [Fig. 2(c)] while RMT predicts significant remaining WL at large B_{\parallel} .

One would expect WL/AL to vanish once orbital effects of B_{\parallel} break time-reversal symmetry. Following

Ref. [12] (FJ), we account for this with a suppression factor $f_{\text{FJ}}(B_{\parallel}) = (1 + \tau_{B_{\parallel}}^{-1}/\tau_{\text{esc}}^{-1})^{-1}$, where $\tau_{B_{\parallel}}^{-1} \sim aB_{\parallel}^2 + bB_{\parallel}^6$, and assume that the combined effects of SO coupling and flux threading by B_{\parallel} can be written as a product, $\delta g(0, B_{\parallel}) = \delta g_{\text{RMT}}(0, B_{\parallel})f_{\text{FJ}}(B_{\parallel})$. The B_{\parallel}^2 term reflects surface roughness or dopant inhomogeneities; the B_{\parallel}^6 term reflects the asymmetry of the quantum well. We either treat a as a single fit parameter (a_1 , Table I), using $b = 1.4 \times 10^8 \text{ s}^{-1} \text{ T}^{-6}$ from device simulations [26], or treat both a and b as fit parameters (a_2 and b_2 , Table I). Fitting both parameters only improves the fit for the (unusually shaped) center-gated dot.

Increased temperature reduces the overall magnitude of δg and also suppresses AL compared to WL, causing AL at 300 mK to become WL by 1.5 K in the $8 \mu\text{m}^2$ dot [Fig. 3(a)]. Fits of RMT to $\delta g(B_{\perp}, 0)$ yield λ_{so} values that are roughly independent of temperature [Fig. 3(b)], and τ_{ϕ} values that decrease with increasing temperature. Dephasing is well described by the empirical form $(\tau_{\phi}[\text{ns}])^{-1} \sim 7.5 \text{ T}[\text{K}] + 2.5 (\text{T}[\text{K}])^2$, consistent with previous measurements in low-SO dots [27]. As dephasing increases, long trajectories that allow large amounts of spin rotations are cut off, diminishing the AL feature.

Finally, we demonstrate *in situ* control of the SO coupling using a center-gated dot. Figure 4 shows the observed crossover from AL to WL as the gate-voltage V_g is tuned from $+0.2 \text{ V}$ to -1 V . At $V_g = -1 \text{ V}$, the region beneath the center gate is fully depleted, giving a

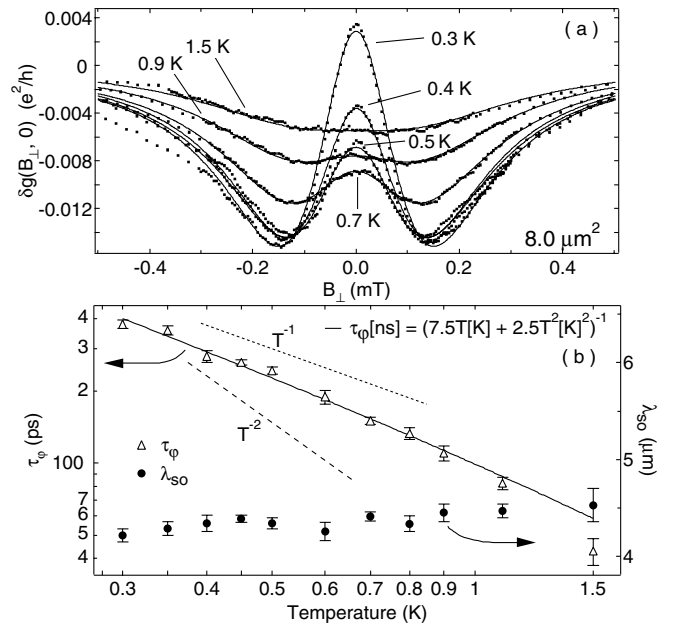


FIG. 3. (a) Difference of average conductance from its value at large B_{\perp} , $\delta g(B_{\perp}, 0)$, for various temperatures with $B_{\parallel} = 0$ for the $8.0 \mu\text{m}^2$ dot (squares), along with RMT fits (solid curves). (b) Spin-orbit lengths λ_{so} (circles) and phase coherence times τ_{ϕ} (triangles) as a function of temperature, from data in (a).

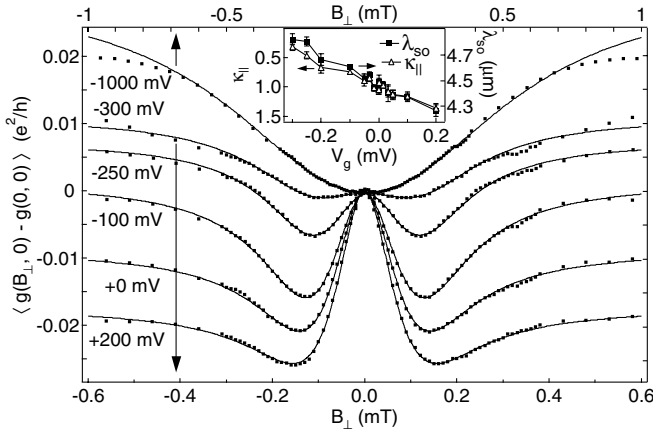


FIG. 4. Difference of average conductance $\langle g \rangle$ from its value at $B_{\perp} = 0$ as a function of B_{\perp} for various center gate voltages V_g in the center-gated dot (squares), along with fits to RMT [5]. Good fits are obtained though the theory assumes homogeneous SO coupling. Error bars are the size of the squares. Inset: λ_{so} and κ_{\parallel} as a function of V_g extracted from RMT fits; see text.

dot with area $5.8 \mu\text{m}^2$ that shows WL. In the range of $V_g \geq -0.3$ V, the amount of AL is controlled by modifying the density under the gate. For $V_g > 0$ V the AL peak is larger than in the ungated $8 \mu\text{m}^2$ dot. We interpret this enhancement not as a removal of the SO suppression due to an inhomogeneous SO coupling [28], which would enhance AL in dots with $L/\lambda_{so} \ll 1$ (not the case for the $8 \mu\text{m}^2$ dot), but rather as the result of increased SO coupling in the higher-density region under the gate when $V_g > 0$ V.

One may wish to use the evolution of WL/AL as a function of V_g to extract SO parameters for the region under the gate. To do so, the dependence may be ascribed to either a gate-dependent λ_{so} or to a gate-dependence of a new parameter $\kappa_{\parallel} = \epsilon_{\parallel}^{so} / \{[(L_1/\lambda_1)^2 + (L_2/\lambda_2)^2] \epsilon_{\perp}^{so}\}$. Both options give equally good agreement with the data [fits in Fig. 4 assume $\lambda_{so}(V_g)$], including the parallel field dependence (not shown). Resulting values for λ_{so} or κ_{\parallel} (assuming the other fixed) are shown in the inset in Fig. 4. We note that the 2D samples from the same wafer did not show gate-voltage dependent SO parameters [10]. However, in the 2D case a cubic Dresselhaus term that is not included in the RMT of Ref. [5] was significant. For this reason, fits using [5] might show $\lambda_{so}(V_g)$ though the 2D case did not. Further investigation of the gate dependence of SO coupling in dots will be the subject of future work.

We thank I. Aleiner, B. Altshuler, P. Brouwer, J. Creemers, V. Falko, J. Folk, B. Halperin, T. Jungwirth, and Y. Lyanda-Geller. This work was supported in part by DARPA-QuIST, DARPA-SpinS, ARO-MURI, and NSF-NSEC. Work at UCSB was supported by QUEST, an NSF Science and Technology Center. J. B. M. acknowledges partial support from NDSEG.

- [1] S. Datta and B. Das, Appl. Phys. Lett. **56**, 665 (1990).
- [2] E. N. Bulgakov *et al.*, Phys. Rev. Lett. **83**, 376 (1999); A. A. Kiselev and K. W. Kim, Appl. Phys. Lett. **78**, 775 (2001); S. Keppeler and R. Winkler, Phys. Rev. Lett. **88**, 46401 (2002).
- [3] A. V. Khaetskii and Y. V. Nazarov, Phys. Rev. B **61**, 12639 (2000); **64**, 125316 (2001).
- [4] B. I. Halperin *et al.*, Phys. Rev. Lett. **86**, 2106 (2001).
- [5] I. L. Aleiner and V. I. Fal'ko, Phys. Rev. Lett. **87**, 256801 (2001); J. N. H. J. Creemers, P. W. Brouwer, I. L. Aleiner, and V. I. Fal'ko (to be published).
- [6] S. Hikami *et al.*, Prog. Theor. Phys. **63**, 707 (1980); B. L. Al'tshuler *et al.*, Sov. Phys. JETP **54**, 411 (1981).
- [7] G. Bergmann, Phys. Rep. **107**, 1 (1984).
- [8] P. D. Dresselhaus *et al.*, Phys. Rev. Lett. **68**, 106 (1992).
- [9] O. Millo *et al.*, Phys. Rev. Lett. **65**, 1494 (1990).
- [10] J. B. Miller, D. M. Zumbühl, C. M. Marcus, Y. B. Lyanda-Geller, K. Campman, and A. C. Gossard, cond-mat/0206375.
- [11] W. Knap *et al.*, Phys. Rev. B **53**, 3912 (1996).
- [12] V. I. Fal'ko and T. Jungwirth, Phys. Rev. B **65**, 81306 (2002); J. S. Meyer *et al.*, Phys. Rev. Lett. **89**, 206601 (2002).
- [13] M. I. D'yakanov and V. I. Perel', Sov. Phys. JETP **33**, 1053 (1971).
- [14] G. Dresselhaus, Phys. Rev. **100**, 580 (1955).
- [15] Y. L. Bychkov and E. I. Rashba, J. Phys. C **17**, 6093 (1983).
- [16] J. P. Heida *et al.*, Phys. Rev. B **57**, 11911 (1988); S. J. Papadakis *et al.*, Science **283**, 2056 (1999); D. Grundler, Phys. Rev. Lett. **84**, 6074 (2000).
- [17] B. Jusserand *et al.*, Phys. Rev. B **51**, 4707 (1995).
- [18] Ç. Kurdak *et al.*, Phys. Rev. B **46**, 6846 (1992); A. G. Aronov and Y. B. Lyanda-Geller, Phys. Rev. Lett. **70**, 343 (1993); A. F. Morpurgo *et al.*, Phys. Rev. Lett. **80**, 1050 (1998); J. Nitta *et al.*, Appl. Phys. Lett. **75**, 695 (1999); H. R. Shea *et al.*, Phys. Rev. Lett. **84**, 4441 (2000); H. A. Engel and D. Loss, Phys. Rev. B **62**, 10238 (2000); A. Braggio *et al.*, Phys. Rev. Lett. **87**, 146802 (2001); F. Mireles and G. Kirczenow, Phys. Rev. B **64**, 24426 (2001).
- [19] B. Hackens *et al.*, Physica (Amsterdam) **12E**, 833 (2002).
- [20] J. A. Folk *et al.*, Phys. Rev. Lett. **86**, 2102 (2001).
- [21] M. Büttiker, Phys. Rev. B **33**, 3020 (1986); H. U. Baranger and P. A. Mello, Phys. Rev. B **51**, 4703 (1995); P. W. Brouwer and C. W. J. Beenakker, Phys. Rev. B **55**, 4695 (1997).
- [22] All measured densities are below the threshold for second subband occupation $n \sim 6.6 \times 10^{15} \text{m}^{-2}$, which is known from Shubnikov-de Haas measurements and a decreasing mobility with increasing density near the threshold.
- [23] I. H. Chan *et al.*, Phys. Rev. Lett. **74**, 3876 (1995).
- [24] D. M. Zumbühl *et al.* (to be published).
- [25] The symmetry is precise if one takes $\epsilon_{\perp}^z = \kappa_z \frac{\epsilon_z^2}{2E_T} \frac{A_z}{\lambda_{so}}$. See Ref. [5].
- [26] V. Falko and T. Jungwirth (private communication).
- [27] A. G. Huibers *et al.*, Phys. Rev. Lett. **81**, 200 (1998); A. G. Huibers *et al.*, Phys. Rev. Lett. **83**, 5090 (1999).
- [28] P. W. Brouwer *et al.*, Phys. Rev. B **65**, 81302 (2002).